Electronic structure and local spectroscopy of 2-D Mott insulators

A Thesis

submitted to

Indian Institute of Science Education and Research Pune
in partial fulfillment of the requirements for the
BS-MS Dual Degree Programme

by

Amitayush Jha Thakur

Indian Institute of Science Education and Research Pune
Dr. Homi Bhabha Road,
Pashan, Pune 411008, INDIA.

April, 2020

Supervisor: Mukul Kabir
© Amitayush Jha Thakur 2020

Certificate

This is to certify that this dissertation entitled *Electronic structure and local spectroscopy of 2-D Mott insulators* towards the partial fulfilment of the BS-MS dual degree programme at the Indian Institute of Science Education and Research, Pune represents study/work carried out by Amitayush Jha Thakur at Indian Institute of Science Education and Research under the supervision of Mukul Kabir, Associate Professor, Department of Physics, during the academic year 2019-2020.

Mukul Kabir   Amitayush Jha Thakur

Committee:

    Mukul Kabir

    Tristan Cren

    Sunil Nair

This thesis is dedicated to my grandfather Dr Chandeshwar Jha

Declaration

I hereby declare that the matter embodied in the report entitled *Electronic structure and local spectroscopy of 2-D Mott insulators*, is the result of the work carried out by me at the Department of Physics, Indian Institute of Science Education and Research, Pune, under the supervision of Mukul Kabir and the same has not been submitted elsewhere for any other degree.

Mukul Kabir   Amitayush Jha Thakur

Acknowledgment

First of all, I would like to express my gratitude to my thesis advisor Dr Mukul Kabir who guided me throughout the project especially in the initial phases when I was trying to get familiar with the world of computational physics. I am also deeply thankful for the opportunity to work at INSP under the guidance of Dr Tristan Cren, who were extremely patient with me and gave me opportunities to experience the fascinating niches in condensed matter physics and get a taste for experimental work. Lastly, I would like to thank Dr Matteo Callandra and Dr Christophe Brun, who were always available to discuss and help me out with any questions I had throughout the course of the project.

x

Abstract

Here we explore the electronic structure of Monolayer Sn/Si(111) $\sqrt{3} \times \sqrt{3}$ R30^0 which is thought to be a correlated 2D Mott insulator. Previous theoretical considerations have indicated that the system might display a row-wise AFM phase or a 120^0 AFM Neel state. Utilizing DFT and DFT+U calculations we compare the various magnetic configurations to identify the ground state configuration for the system which turns out to be in a row-wise AFM order. The mechanism behind the insulating behaviour can be attributed to be either a weak correlation driven Slater insulator or a true strongly correlated Mott insulator. We show that the system is most likely to be a Slater insulator from our calculations. By examining the core level electronic spectra we are also able to provide an explanation for the 2 double peaks seen in the core level ARPES spectra. Finally, we are able to observe a doping driven insulator to metal transition and calculate the electronic structure and magnetic configuration of these possible doped states.

Contents

Introduction

Strongly correlated systems have become a cornerstone of condensed matter physics in recent years. This field gained prominence and caught the interest of the community after the discovery of high temperature superconductivity in 1980s[1]. This discovery brought a whole host of new problems involving physics which couldn't be explained by actions of individual particle like entities and have to be treated with keeping the collective interactions of electrons in mind. This renewed interest was also accompanied with a surge in the computational capabilities and development of methods attempting to gain insights into the electronic properties of materials.

The study of 2-D materials has also been growing in prominence after the isolation of graphene in 2004 [2] which gave the community the opportunity to experimentally study the role of dimensionality in the structural and electronic properties of material. 2-D also provides us with an ideal ground to study systems with electronic correlation as well as studying phase transitions and competing phases. This is due to the increase in competition between entropy change and internal energy in 2-D compared to 3-D where entropy usually dictates the nature of phase space. Such correlated behaviour usually involve the d or f orbital which have shown a propensity for being localized and thus showing strong electronic interaction. Therefore materials involving transition metals , lanthanides and such like transition metal dichalcogenides (TMD) have been the focus of research in this area. However another class of materials involving metal adsorbates on semiconductor surface have emerged as a platform to study electronic correlations. The coverage of the adsorbate can be controlled precisely to form phases where electronic correlation effects begin to dominate.

The 1/3 ML Sn/Si(111) is an example of such a material and the focus of this theses. This material is also special because photoemission [3] and scanning tunneling spectroscopy (STS) [4] experiments have found this material to be insulating which is not expected because of the

half filled band inside the semiconducting band gap. This insulating behaviour is attributed to the presence of electronic correlations and thus this material is predicted to be a Mott insulator. This material is also exciting as recently hole doped 1/3 ML Sn/Si(111) has shown supercoductivity [5] at a T_c of around 4.5K which is even exceeds that of bulk Sn (T_c = 3.7K). The study seems to suggest that the mechanism of action might be similar to that found in high temperature unconventional superconductors. If this is indeed the case, a study of this simpler material might help us gain valuable insights into unconventional superconductivity in the complex layered superconductors.

Density functional theory (DFT) has been employed to solve solid-state problems since the 1970s but still has been largely unsuccessful in dealing with materials involving strong interactions. DFT+U has been put forward as a tool to incorporate some elements of the many body interaction in the simple DFT framework and has found relative success in describing materials like TiO_2 [6], Ce_2O_3 cite7 and various organometallics [8] where DFT has traditionally failed.

In this study we employ DFT and DFT+U based methods to identify the correct ground state and magnetic properties of the 1/3 ML Sn/Si(111) correlated material and investigate the nature and extent of correlation effects based on these calculation. We also try to prepare the actual samples and image them using a scanning tunneling microscope.

Chapter 1

Theory

1.1 Density functional theory

Density functional theory (DFT) is the backbone of this project. It is a very powerful computational tool for ab-initio calculation of electronic structure of many body systmems. The foundations of the theory lie in two theorems proved by Walter Kohn and Pierre Hohenberg known as the Hohenberg-Kohn (H-K) theorems [8]. These theorems are given as :

- Theorem 1: For any system of interacting particles in an external potential V(r), the V(r) is determined uniquely, except for a constant, by the ground state particle density n(r).

- Theorem 2: A universal functional for the energy E[n] in terms of the density n(r) can be defined, valid for any external potential V(r). For any particular V(r), the exact ground state energy of the system is the global minimum value of this functional, and the density that minimizes the functional is the exact ground state density n(r).

Based on these theorems an energy functional in terms of electron density can be constructed .

$$E_{HK} = T[n] + E_{int}[n] + \int d^3 r V_{ext}(r) n(r) + E_{II} \tag{1.1}$$

Where the terms $T[n]$ is the kinetic energy contribution and E_{int} the interaction between

the electrons $\int d^3 r V_{ext}(r) n(r)$ the interaction energy between the nucleus and the electrons and E_{II} is the interaction between the nuclei the many body system.

The problem appears to be simplified on the surface owing to a simple term n(r) instead of equations for individual electrons but it is still intractable as it involves many body interactions which can't be solved analytically. To solve this problem a different framework was introduced by Walter Kohn and Lu Jeu Sham which reduced this problem to a system of non-interacting electrons acting in an effective potential [9]. The H-K functional written in the Kohn-Sham (K-S) framework is ,

$$E_{KS} = T_s[n] + \int d^3 r V_{ext}(r) n(r) + E_{Hartree}[n] + E_{II} + E_{XC}[n] \tag{1.2}$$

Where

$$T_s = -\frac{1}{2} \sum_\sigma \sum_{i=1}^{N^\sigma} <\psi_i^\sigma | \nabla^2 | \psi_i^\sigma> = \frac{1}{2} \sum_\sigma \sum_{i=1}^{N^\sigma} \int d^3 r |\nabla \psi_i^\sigma(r)|^2 \tag{1.3}$$

is the single particle kinetic energy in terms of the single particle wavefunctions ψ_i^σ and

$$E_{Hartree} = \frac{1}{2} \int d^3 r d^3 r' \frac{n(r) n(r')}{|r - r'|} \tag{1.4}$$

is the direct coulomb interaction and E_{XC} includes the many body exchange interaction and correlations which is now approximated to solve the full system.

Now minimizing the K-S functional w.r.t the wavefunction we can arrive at Schrodinger-like equations given by

$$(H_{KS}^\sigma - \varepsilon_i^\sigma) \psi_i^\sigma(r) = 0 \tag{1.5}$$

where ε_i^σ are the K-S eigenvalues and

$$H_{KS}^\sigma = -\frac{1}{2} \nabla^2 + V_{KS}^\sigma \tag{1.6}$$

$$V_{KS}^\sigma = V_{ext}(r) + \frac{\partial E_{Hartree}}{\partial n(r, \sigma)} + \frac{\partial E_{XC}}{\partial n(r, \sigma)} = V_{ext}(r) + V_{Hartree}(r) + V_{XC}(r) \tag{1.7}$$

Now these equations can be solved in a self consistent manner according to 1.2. Note that our solutions are only as good as our approximations for E_{XC}. The most popular approximation for E_{XC} is the local density approximation (LDA) where the functional depends only on the

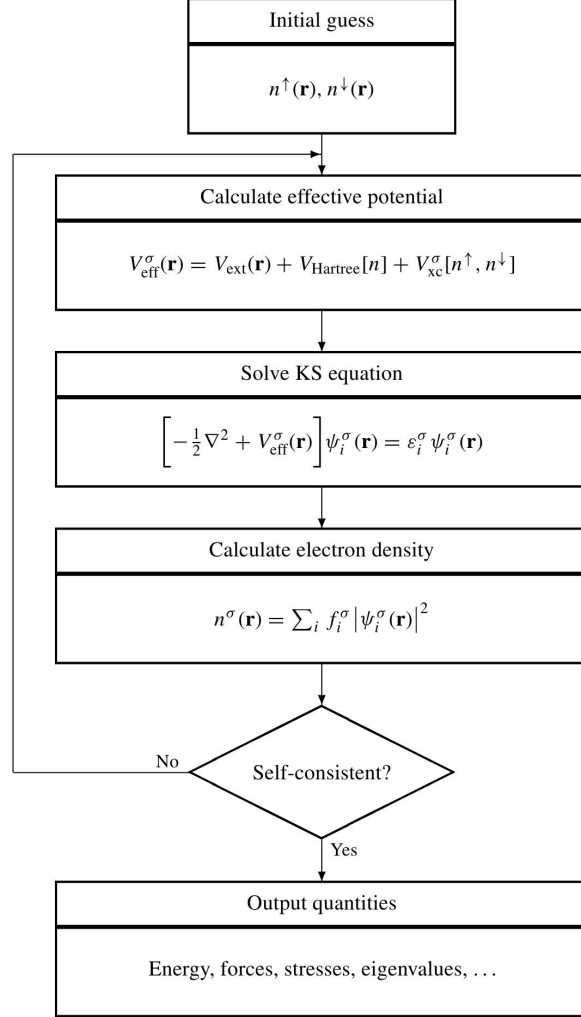**Self-consistent Kohn–Sham equations**

Figure 1.1: From [11]. Schematic representation of the self-consistent loop for solution of Kohn–Sham equations.

local density of electrons,

$$E_{XC}^{LDA} = \int \varepsilon_{XC}(n)n(r)d^3r \tag{1.8}$$

In our work we extensively utilized Perdew–Burke-Ernzerho (PBE) [10] functional which is a type of generalized gradient approximation (GGA) functional which also includes the gradient of electron density and takes into account the potential non-homogeneity of the

electron density. The general form can be written as ,

$$E_{XC}^{GGA} = \int \varepsilon_{XC}(n, \nabla n)n(r)d^3r \tag{1.9}$$

1.2 DFT+U

1.2.1 Hubbard model and LDA+U

Density functional theory has proven to be very successful in describing systems where the electronic interactions are not strong and system has well defined quasiparticle like ex citations. However it fails quite heavily to successfully capture the behaviour of systems where strong electronic interactions dictate the electronic structure. An example of such a system is a Mott insulator [12][13] where the coulomb interactions are so strong that electrons become localized to specific orbitals. DFT functionals like LDA and GGA generally tend to over delocalize the valence orbitals and tend to stabilize a metallic ground state and hence fails to capture the physics of strong correlations due to localization.

To understand the phenomenon of electronic correlations and localization we employ a fairly simple model called the Hubbard Model where a simple one band Hamiltonian is given as ,

$$H_{Hub} = t \sum_{<i,j>,\sigma} (c_{i,\sigma}^\dagger c_{j,\sigma} + h.c) + U \sum_i n_{i,\uparrow} n_{i,\downarrow} \tag{1.10}$$

Here the sum involves only nearest neighbours i,j , $c_{i,\sigma}^\dagger, c_{j,\sigma}$ are the electron creation and annihilation operators at site i and j respectively and $n_{i,\sigma}$ are the number operators for electrons at site i and spin σ. The parameter t controls the hopping of electrons between sites i and j and is proportional to the bandwidth while the term U takes care of the on-site coulomb interaction when electrons of opposite spin are present at the same site. If t $\ll$ U ,i.e there is a huge cost associated with putting the electrons on the same site and the hopping cannot overcome this coulomb repulsion we get an insulator even with a half filled band which would have been predicted to be a conductor by electron counting. This behaviour is not correctly described by DFT which can normally account for the other limit U $\ll$ t (where system behaves like having well defined quasiparticles) quite well.

6

While there exists some many-body methods like DMFT (dynamical mean field theory) [14] and cluster approximations [15] which can capture such strongly correlated behaviour ,the simplicity and computationally low cost of DFT encourages us to find a way to incorporate features of such behaviour in it. This gives rise to the LDA+U approximation [16](which can be extended to other functionals also and generally called DFT+U) . Within LDA+U , the energy functional is given as

$$E_{LDA+U}[\rho(r)] = E_{LDA}[\rho(r)] + E_{Hub}[n^{I\sigma}_{mm'}] - E_{dc}[n^{I\sigma}] \qquad (1.11)$$

here , E_{Hub} contains the electron-electron interaction according to the Hubbard Hamiltonian and E_{dc} is the double counting term which removes the interaction energy already present in E_{LDA} to avoid problems due to double counting. $n^{I\sigma}_{mm'}$ are the occupation numbers of the localized orbitals and are defined as ,

$$n^{I\sigma}_{mm'} = \sum_{k,v} f^{\sigma}_{kv} < \psi^{\sigma}_{kv}|\phi^{I,\sigma}_{m'} >< \phi^{I,\sigma}_{m}|\psi^{\sigma}_{kv} > \qquad (1.12)$$

where ψ^{σ}_{kv} are the K-S orbitals and $\phi^{I,\sigma}_{m}$ are the states of localized basis set. According to [18] the total Hubbard correction $E_U = E_{Hub} - E_{dc}$ can be given by

$$E_U[\{n^{I\sigma}_{mm'}\}] = \sum_{I,\sigma} \frac{U^I}{2} Tr[\mathbf{n}^{\mathbf{I},\sigma}(1 - \mathbf{n}^{\mathbf{I},\sigma})] \qquad (1.13)$$

1.2.2   Calculation of U using linear response method [17]

Generally a value of U is approximated by comparing with the experiments and fitting a parameter to match certain properties and is not known a-priori. However depending on the system's properties including structure and magnetism this value is not fixed and therefore, should be calculated for a given system to gain some predictive power while working with correlated systems.

The total energy given by DFT is an approximately analytic function of electron occupancy of the orbitals. However , it should instead be a series a straight line segments which match with the analytic curve at integer occupancy [19, 20, 21]. This piece-wise linear correction has the form of eq. 13 if we take the value of U to be the curvature of this function. Therefore U can be calculated as the second derivative of energy as a function of electron
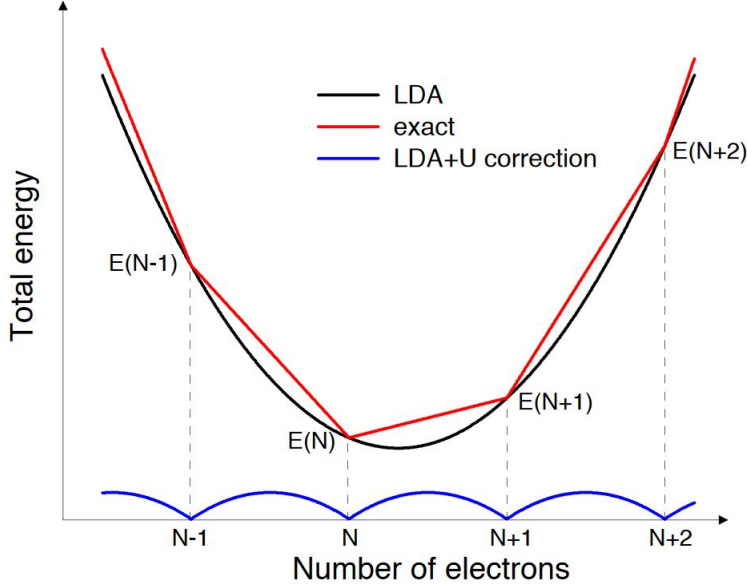
Figure 1.2: From [17]. Schematic representation of the DFT total energy as a function of electron occupation. Red line represents the exact energy, black line the DFT energy and blue line represents the difference between the two.

occupancy which recovers the physical behaviour of the DFT energy function. This value is calculated by utilizing a small perturbation to the K-S potential which is proportional to the projector on the localized states of atom I.

$$V_{tot}|\psi_{kv}^{\sigma}> = V_{KS}|\psi_{kv}^{\sigma}> +\alpha^I \sum_m |\phi_m^I><\phi_m^I|\psi_{kv}^{\sigma}> \qquad (1.14)$$

For the modified K-S energy functional the ground state if α dependent and is given by

$$E(\alpha^I) = \min_{\eta}(E_{DFT}(\eta) + \alpha^I n^I) \qquad (1.15)$$

where η is the one body density matrix. We can write $E[\{n^I\}] = E(\alpha^I) - \alpha^I n^I$ for electron occupancy n^I at the minima of above equation. Therefore we get $d^2E/d(n^I)^2 = -d\alpha/dn^I$. If we vary α^I and record the variation in all n_J we obtain a response matrix $\chi_{IJ} = dn^J/d\alpha^I$ (I and J are the sites of Hubbard atoms). The inverse of this response matrix gives the value of Hubbard U, $U^I = -\chi_{II}^{-1}$. An extra term which measures the rehybridization of the wavefunctions in response to perturbation has to be subtracted out which is given by χ_0. Therefore, the linear response value of Hubbard U is given by $U^I = (\chi_0^{-1} - \chi^{-1})_{II}$.

8

1.3 Mechanisms for Insulating behaviour

The various mechanism behind insulating behaviour of a solid can be summarized as follows:

- **Band Insulator** : This can be understood by using a simple 1-D tight binding model where the the Hamiltonian is given as,

$$H_{tbh} = -t \sum_{<j,i>\sigma} ((c_{1,\sigma}^\dagger c_{j,\sigma} + h.c) - \mu \sum_j (n_{j\uparrow} + n_{j\downarrow}) \tag{1.16}$$

where $c_{i,\sigma}^\dagger, c_{j,\sigma}$ are the electron creation and annihilation operators at sites i and j respectively. This can be solved by going to momentum state operators and we get the diagonal hamiltonian as ,

$$H = -2t \sum_{k\sigma} cos(k) c_{k\sigma}^\dagger c_{k\sigma} = \sum_{k\sigma} \varepsilon_k n_{k\sigma} \tag{1.17}$$

where $c_{k\sigma}^\dagger = \frac{1}{\sqrt{N}} \sum_j e^{i\mathbf{k.j}} c_{j\sigma}^\dagger$ is the momentum space fermionic operators. Therefore we get a continuous tight banding band. Now if we introduce a staggered potential $\Delta \sum_j (-1)^j n_{j\sigma}$ in the Hamiltonian we actually open a gap at momenta $k = \pm\pi/2$ and the energy dispersion is now given by ,

$$E_k = \pm\sqrt{\varepsilon_k^2 + \Delta^2} \tag{1.18}$$

Instead of a staggered potential ,if multiple fermionic species are present ,depending on the relative strength of the hopping parameter we can also get insulating behaviour.

- **Spin density wave** : Consider the Hubbard Hamiltonian

$$H_{Hub} = -t \sum_{<j,i>\sigma} ((c_{1,\sigma}^\dagger c_{j,\sigma} + h.c) - \mu \sum_j (n_{j\uparrow} + n_{j\downarrow}) + U \sum_j n_{j\uparrow} n_{j\downarrow} \tag{1.19}$$

Using mean field approximation the Hubbard term can be written as,

$$U \sum_j (n_{j\uparrow} < n_{j\downarrow} > + n_{j\downarrow} < n_{j\uparrow} > - < n_{j\uparrow} >< n_{j\downarrow} >) \tag{1.20}$$

If we consider an antiferromagnetic (AFM) pattern for electron occupation $< n_{j\uparrow} >=$

$\eta + (-1)^j m$ and $< n_{j\downarrow} >= \eta - (-1)^j m$ ensuring physical value of occupation ,we get a very similar case of tight binding Hamiltonian in a staggered potential as before and an insulating gap opens up. This type of spin density wave AFM insulator in relatively weak Coulomb repulsion is also known as Slater insulator.

- **Charge density wave** : In this case electrons interact primarily through phonon modes and the Hamiltonian known as the Holstein Hamiltonian can be written as ,

$$H_{Holstein} = -t \sum_{<j,i>\sigma} ((c^{\dagger}_{1,\sigma}c_{j,\sigma} + h.c) + \frac{1}{2}\sum_{j}(p_j^2 + \omega^2 q_j^2) + \lambda \sum_{j}(n_{j\uparrow} + n_{j\downarrow})q_j \quad (1.21)$$

where p_j and q_j are the phonon momentum and displacement operators. Now, if we ignore the phonon kinetic energy and consider an oscillating displacement $< q_j >= (-1)^j q_0$ we again get a tight binding model with a staggered potential and an insulating gap appears.

- **Mott Localization** : Consider equation 2.19. At intermediate value of U we expect that an AFM order is stabilized as electrons of opposite spin can travel near each other and lower the energy of the system by t^2/U (second order energy approximation). However, if if t $\lll$ U this movement of electrons becomes more constrained and there comes a point where the system can be insulating without any apparant magnetic order. This localization at strong correlations results in the Mott insulator.

- **Anderson Localization** : This type of localization occurs due to randomness or defects in the tight binding Hamiltonian. Solving the tight binding Hamiltonian in presence of defects result in the formation of localized wavefunctions at the site of the defect and if the presence of such localized wavefunctions is sufficient enough this can hinder the movement of the band electrons and open up an insulating gap.

Chapter 2

Experimental Concepts

2.1 Low Energy Electron Diffraction (LEED)

Low energy electron diffraction (LEED) is a widely used technique to probe the surface structure of a crytalline material. The typical energy of electrons range from 20-200eV.

2.1.1 Theory

The low energy of electrons involved ensures that only the surface structure is probed by the electron beam. If only elastic scattering is ensured the magnitude of incident electron wavevector $\mathbf{k_0}$ is equal to the the scattered wavevector $\mathbf{k}$. Now, as only the surface electrons contribute to the scattering and there is no scattering in the perpendicular direction to the surface and the Laue Condition [22] can be given as an

$$\mathbf{k}^{||} - \mathbf{k_0}^{||} = G_{hk} = ha^* + kb^* \tag{2.1}$$

where a^* and b^* are the reciprocal space primitice lattice vectors of the real surface lattice. This can be visualised using the Ewalds sphere [23] (fig 2.1). The lattice points perpendicular to surface from a continuous rod as there is no diffraction condition in that direction. In this way LEED allows us to directly probe the surface organization and allows us to easily keep track of the surface reconstructions during the preparation of the sample.
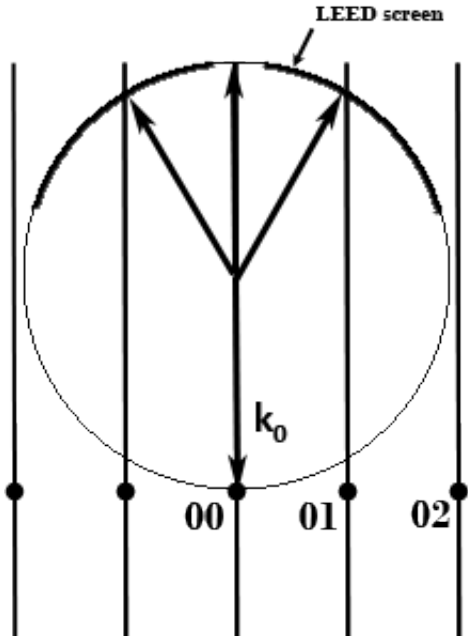
Figure 2.1: Ewalds sphere construction. The numbers indicate the value of h and k for the diffracted beam

2.1.2 Experimental Setup

Figure 2.2 shows a schematic of a LEED setup. The electron gun fires a beam of electrons at the sample and the backscattered electrons which are elastically scattered reflect back towards the fluorescent screen and from the pattern of the surface reciprocal lattice. To ensure that only elastically scattered electrons are collected a series of grids are used to slow down and scatter away low energy electrons.

2.2 Scanning Tunneling Microscopy (STM)

2.2.1 Theory

The operating principal behind STM is the phenomena of electron tunneling through a barrier. A simple 1-D Schrodinger equation in presence of a potential barrier U(z) can be
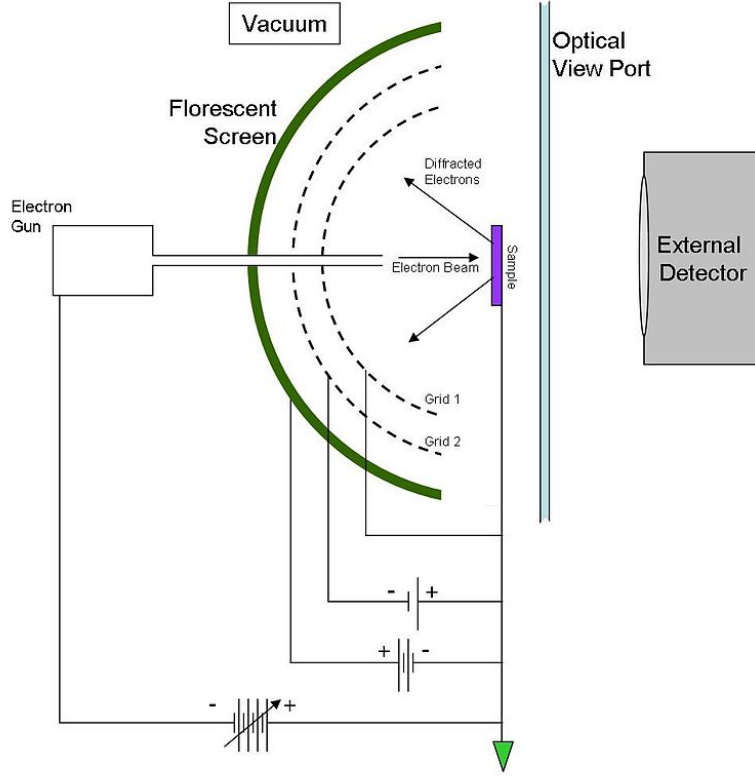
Figure 2.2: A schematic showing the basic setup of a LEED device.[33]

written as ,

$$-\frac{\hbar}{2m}\frac{\partial^2 \psi_n(z)}{\partial z^2} + U(z)\psi_n(z) = E\psi_n(z) \tag{2.2}$$

In the classically forbidden region we have exponential decay of the wavefunction and $\psi_n(z) = \psi_n(0)e^{\pm kz}$ where $k = \sqrt{2m(U-E)/\hbar^2}$. Extending this idea to a sample-vacuum-tip interface in real life applications , the tunneling current I_{tip} is found to be proportional to e^{-2zk} and k is now equal to $k = \sqrt{2m\phi/\hbar^2}$ where ϕ is the work function of the surface and the bias is small enough so that only the states near Fermi level are probed. Therefore, due to the exponential response of the tunneling current, STM is very sensitive to surface changes in the z direction. The STM can be operated in two primary modes based on the control of operating parameters.

- Constant current mode, where the tunneling current is kept constant by the feedback mechanism, i.e. if the tip and the sample are too far apart and the tunneling current

13

decreases, the feedback mechanism will bring the tip closer to the surface to increase the current to the defined constant value. By tracking the movement of the tip, we obtain a topographic image of the surface by this method.

- Constant height mode, where the height of the tip above the surface is kept constant (i.e the feedback mechanism controlling the tip height is turned off) and the changes in the tunneling current as the tip moves over the sample are tracked. If the sample is completely flat, this method allows to map the local density of states (DOS) of the sample surface if we also vary the bias at every point. We can thus obtain a dI/dV map which is proportional to the local DOS.
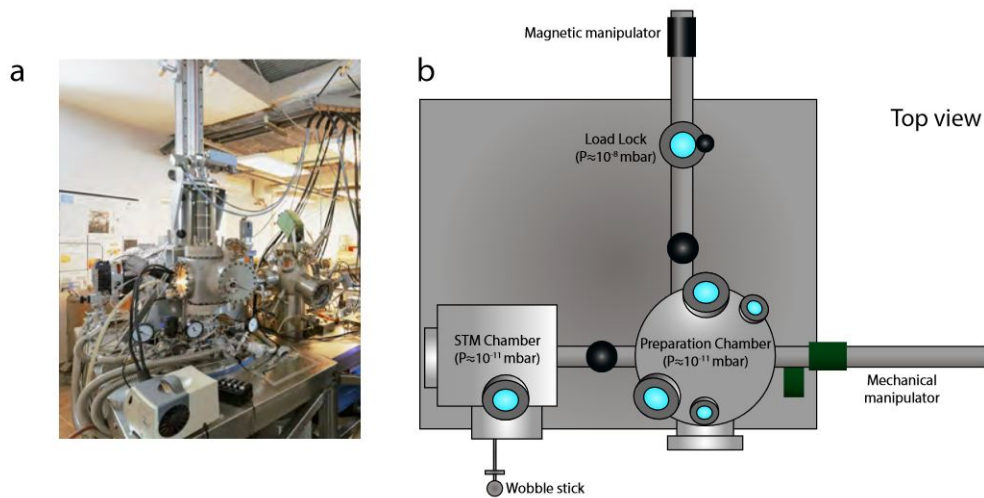
2.2.2 Experimental Setup

Figure 2.3: a) The experimental setup . b) A schematic depicting the various chambers and components of the setup . From [34].

The setup is shown in figure:STM. The STM consists of three main chambers, the load-lock chamber which is used to transfer tips and sample into the STM, the preparation chamber which houses the electron beam evaporator and the quartz microbalance. We can also attach the LEED and Auger devices to this chamber which allows us to prepare the necessary samples in-situ. The STM chamber is able to operate at temperature upto 300mK , has a base pressure of 10^{-11}mbar at room temperature and work with magnetic fields upto 7T. WSxM [24] software was used to obtain the topographic images.

Chapter 3

The Sn/Si(111) surface

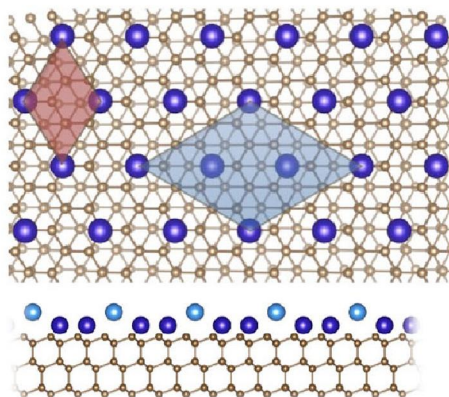## 3.1   Tetravalent adatoms on Semiconductor Surfaces

Figure 3.1: Top and side view of the charge ordered 1/3 ML Pb/Si(111) surface. Red and blue highlighted areas represent the $\sqrt{3} \times \sqrt{3}$ and 3×3 reconstruction respectively. The up-down Pb atoms of the 3×3 can be visualized in the side view. From [27]

1/3 ML Sn/Si(111) belongs to a family of surfaces with similar isoelectronic phases like Pb/Si(111), Pb/Ge(111), Sn/Ge(111) and Sn/SiC(0001). At 1/3 ML coverage these adatoms saturate three Si atoms each but are left with an unsaturated electron which results in a half filled band in the semiconducting gap. However, a small class of these materials like the Sn/Si [3, 4] and Sn/SiC [25] have been found to be insulating and have been classified as Mott insulators.

All of these systems show a $\sqrt{3} \times \sqrt{3}$ reconstruction at room temperature. Several studies to investigate the nature of these systems at low temperature have been conducted which reveal that some systems like Pb/Ge(111), Pb/Si(111) and Sn/Ge(111) transition to a charge ordered 3×3 phases with distortions of the adsorbed atom perpendicular to the surface [26, 27, 28]. The Sn/Ge(111) system also shows such a charge ordered phase but goes back to a $\sqrt{3} \times \sqrt{3}$ phase with insulating behaviour at still lower temperatures.

3.2   1/3 ML Sn/Si(111)

As discussed earlier, at room temperature this system exists in a stable $\sqrt{3} \times \sqrt{3}$ with the Sn atoms being located at the T4 sites above the second layer Si atoms does not show any sign of transition to a different reconstruction at lower temperatures [4]. STM measurements have indicated a Mott transition at a temperature between 30 to 40K with an insulating gap of around 70 meV [29]. As an insulating gap is often occompanied by some magnetic transition, an investigation of magnetic order at low temperature is very important for understanding the electronic structure of this system. However, no direct magnetic measurements as of yet, have been performed on this system. Theoretical considerations have indicated that the system might display a row-wise AFM phase or a 120^0 AFM Neel state (In plane triagonal order in this theses) [21]. A recent ARPES study [3] has claimed to provide evidence for the row wise AFM order but the insulating gap reported in the ARPES studies is much larger than the ones found in the STS studies.
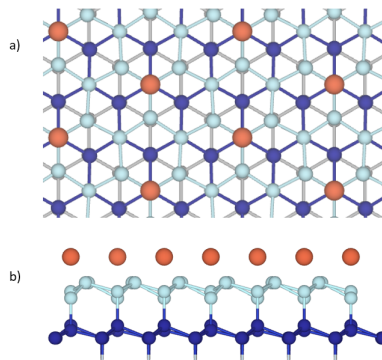

Figure 3.2: Top and side view of the 1/3 ML Sn/Si(111) surface. Red balls depict the Sn atoms at T4 sites while the light blue and dark blue balls represent Si atoms in the first and second bilayer from the top.

Chapter 4

Results

4.1 Density functional theory based calculations

4.1.1 Optimization of the initial structure

All calculations were based on QUANTUM ESPRESSO [30] code. It utilizes plane waves basis set and are thus quite suited for calculations involving periodic crystal like structure. The initial supercell consisted of a Si(111) surface with 3 silicon bilayers with hydrogen atoms bonded to the dangling electrons of the bottom Si surface and around 16 Å of vacuum to simulate a slab and prevent interactions between the slabs in z direction. The Sn atoms were then placed at T4 positions above the Si(111) surface and the position of the atoms of the top two Si bilayers along with the Sn atoms was optimized to reduce any residual forces introduced by adding the Sn atoms. Calculations were mainly done using a GGA exchange-correlation functional (PBE) and using an ultrasoft pseudopotential with an energy cutoff of 45 Ry.

4.1.2 The $\sqrt{3} \times \sqrt{3}$ supercell

The $\sqrt{3} \times \sqrt{3}$ supercell was constructed with one Sn atom per supercell. The paramagnetic calculations showed a clearly isolated surface band in the bulk bandgap. However we see
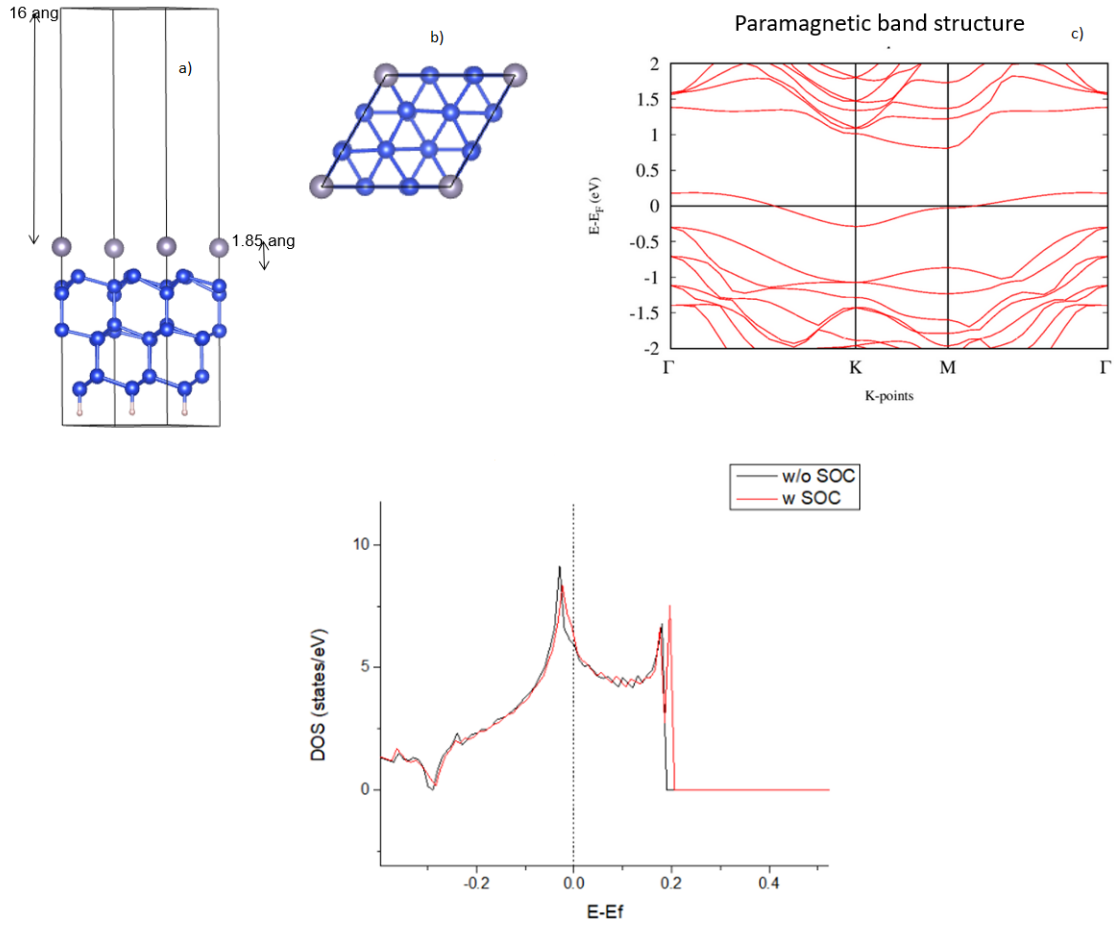
Figure 4.1: Top: a) The side view of the $\sqrt{3} \times \sqrt{3}$ supercell with 16 Å of vacuum to stimulate the 2D slab like model. b) Top view of the supercell c) Paramagnetic band structure. Bottom: The paramagnetic DOS with and without SOC. SOC only causes a band splitting of 20meV or 5% of the total band.

the surface band is conducting which is in clear contradiction to the experimental data [29], therefore a simple paramagnetic (PM) model is unable to accurately describe our system. Spin orbit coupling (SOC) was then implemented in our system using relativistic pseudopotentials but we observe only a 5% SOC splitting therefore we don't include any relativistic effects in further calculations.
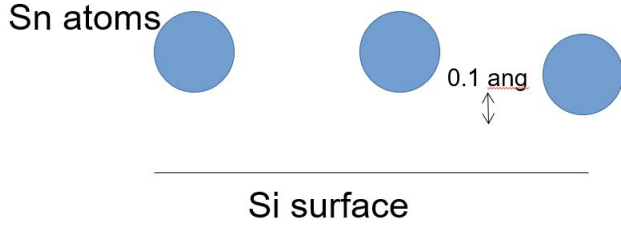
Figure 4.2: Cartoon representation of the up-down order found to be stabilized in presence of collinear magnetism.

4.1.3 The 3×3 supercell

A possible charge ordered 3×3 reconstruction was investigated (similar to the blue highlited zone in Fig. 3.1) which have been found to be stable in some similar correlated surfaces like 1/3 ML Pb/Si(111) [27]. The paramagnetic calculations of the electronic structure of a 3×3 supercell with 3 Sn atoms don't reveal a charge ordered phase but a collinear ferrimagnetic magnetic order with out of plane magnetization of the Sn atoms does stabilize a phase with 2 Sn atoms about 0.1 Å above than the third one as shown in 4.2.

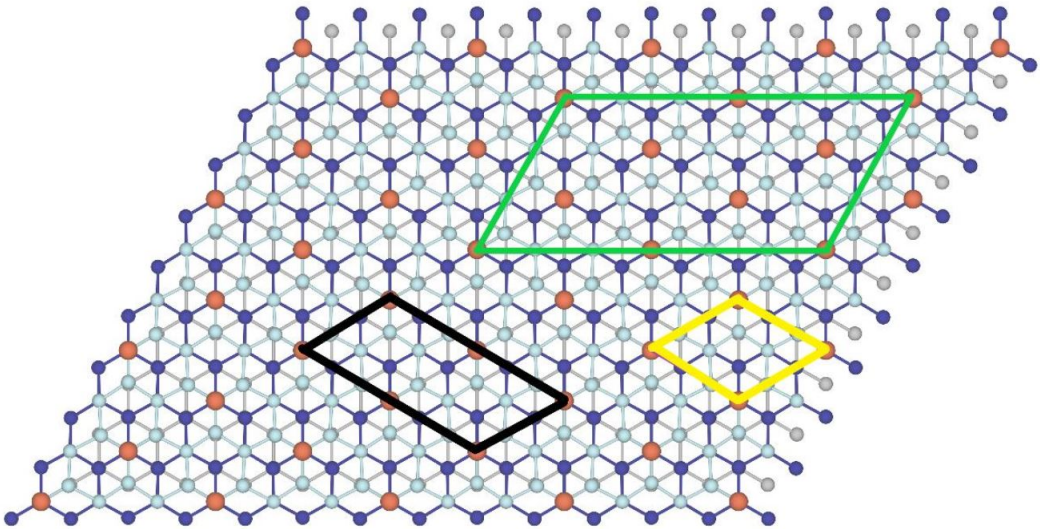### 4.1.4 Investigation of the magnetic order

Figure 4.3: The supercells used in DFT calculations. 6×3 cell is green, the $\sqrt{3} \times \sqrt{3}$ cell in in yellow and the $2\sqrt{3} \times \sqrt{3}$ cell is depicted in brown.
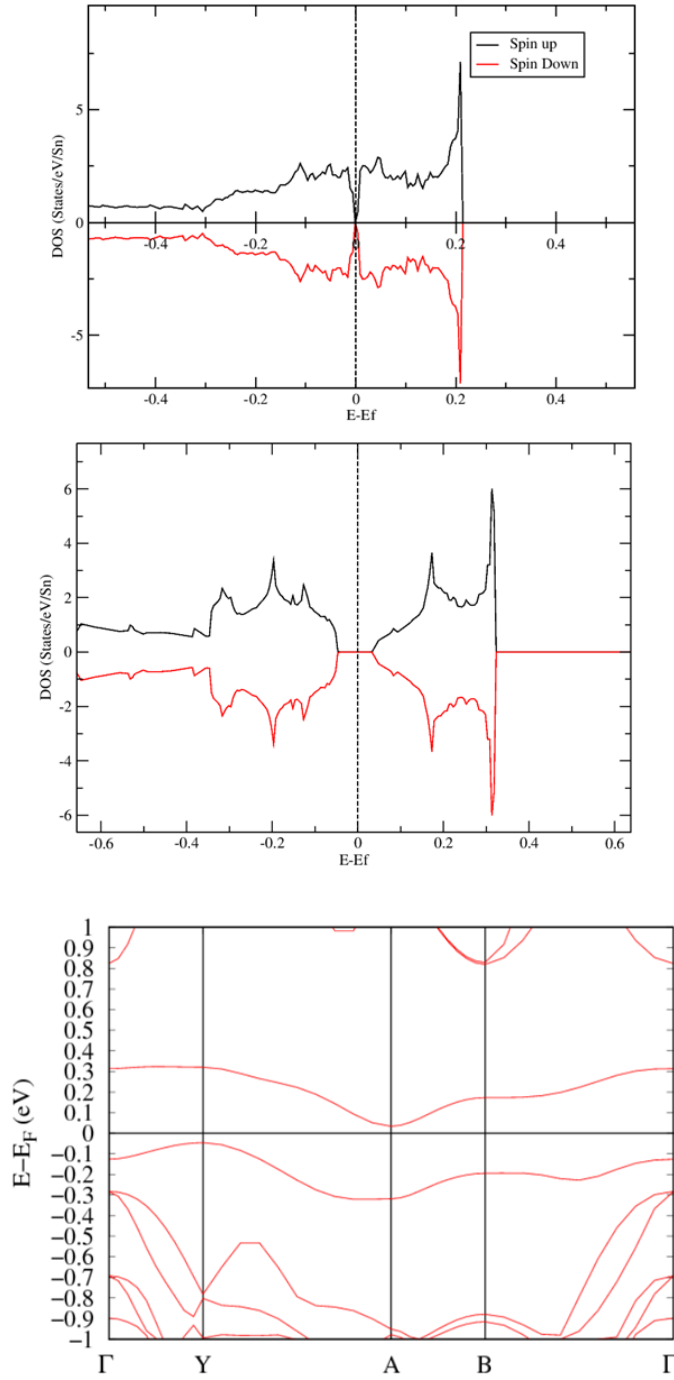
Figure 4.4: Top: DOS of row-wise AFM configuration without any U. Middle: DOS in the presence of U=2.12 eV with a gap of 70meV. Bottom: Band structure of the AFM configuration $(2\sqrt{3} \times \sqrt{3}$ supercell) with U.

The potential for magnetic ground state was investigated next. The $\sqrt{3} \times \sqrt{3}$ supercell only has one Sn atom per supercell, therefore to investigate competing magnetic orders a bigger supercell was needed. The possibility of a row-wise antiferromagnetic (AFM) order has been suggested by earlier investigations [29], therefore a $2\sqrt{3} \times 2\sqrt{3}$ supercell was constructed with 4 Sn atoms and a row-wise AFM order. The density of states (DOS) at the fermi level is sharply depleted and see an apparent stabilization of the AFM order compared to the paramagnetic order which qualitatively matches some earlier experimental studies[4]. To accurately compare the ground state energetics of the various magnetic states. Figure 4.5 shows the various magnetic orders studied.

The calculations reveal that the AFM phase is indeed the most stable one with a magnetic moment of magnitude 0.05 μB . Inspite of being the most stable magnetic configuration in our calculation and showing a strong depletion of DOS at the fermi level we don't really see a insulating gap in our calculations as seen in the experimental studies. To improve our calculations and enhance the effects of correlations in our system a rotationally invariant formulation of DFT+U approximation was used [18]. The self consistent value of U was calculated to be 2.12 eV using the linear response method [17]. The p-orbital of the Sn atom with its dangling electrons was subject to the on-site Hubbard repulsion as it is identified to be most likely to localized at the surface.

The various magnetic structures were all then also studied in a 6×3 unit cell to get an accurate comparison of the energies.In addition to the collinear out of plane magnetic orders we also include some in plane magnetic order like the 120° inplane anti-ferromagnetic order which is also touted as a possible ground state for the system [21] along with a seemingly irregular inplane magnetic order which occurs out of stabilization of some inplane magnetic calculations. This irregular magnetic order is recognized to be the incomplete stabilization of an inplane row-wise AFM order and it matches very closely in energy with the out of plane row-wise AFM order. The charge ordered phase which appeared with the 3×3 order also disappeared upon stabilization in presence of U and therefore was not considered for further calculations.

The DFT+U calculations show that the row-wise AFM phase is still the most stable configuration of the ones studied and the Hubbard U makes the energy difference more pronounced which imply an important consequence of adding the on-site coulomb repulsion. The energy gap is around 70 meV and this is of the order of the energy gap found in STS

experiments [29] .

Mag. config	AFM	FIM	FM	PM
ΔE/Sn	0.000	0.042	1.683	2.610
Mag.Moment	0.0519	0.0267,-0.0508	0.0208	0.000

Table 4.1: Energy of collinear magnetic configurations using PBE functional(GGA). The ΔE/Sn values are the energy difference (in meV) w.r.t the AFM configuration. The Mag. Moment is the magnitude of on site Sn magnetic moment (in μB). The magnitude of the spin up and spin down Sn atoms are listed separately of the case of FIM.

Mag. config	AFM	FM	IP TRI	IP AFM
ΔE/Sn	0.000	16.669	0.171	0.071
Mag.Moment	0.0908	0.0841	0.085	0.0970

Table 4.2: Energy of collinear magnetic configurations using PBE+U.The value of U is 2.1 eV. The ΔE/Sn values are the energy difference (in meV) w.r.t the AFM configuration. The Mag. Moment is the magnitude of on site Sn magnetic moment (in μB).

4.1.5   Characterization of the surface band

Orbital resolving the surface band reveals that it has about 65% Si p orbital ,24% Sn p orbital, 5% Si s orbital and 4% Sn s orbital character. This suggests that the Sn adatoms are heavily hybridized with the Si atoms underneath. Indeed, resolving the surface band according to the contributing Si bilayers in case of the most stable AFM configuration reveal that there is non-trivial contributions of the bulk Si atoms to this band . This hybridization is more clearly seen by plotting the localized Wannier wavefunction .

4.1.6   Calculation of magnetic exchange strength

If we assume that the electrons are localized sufficiently we can map the energy of interactions between the the magnetic atoms with an Ising hamiltonian which is given by

$$H_{ising} = -\frac{1}{2} \sum_{<i,j>} J_{ij} S_i S_j \tag{4.1}$$

Here the sum over i,j involves only nearest neighbour i.e the superexchange interaction is short ranged , $J_{ij} = J$, the exchange coupling is homogeneous over the lattice and S_i, S_j are the magnetic moments at site i j. We can relate the energy difference of the FM and AFM configuration to the the strength of the exchange coupling if we assume the Ising type magnetic interaction .The magnetic energy of the FM configuration in the 6×3 supercell is given as $-7JS_z^2$ and of the AFM configuration is given by $3JS_z^2$.

$$\Delta E = E_{AFM} - E_{FM} = 10JS_z^2 \tag{4.2}$$

Assuming S_z to be 1/2 we get the exchange strength of the system with and without Hubbard U as -0.040 eV and -0.004 eV respectively. So we see that in the case of DFT+U calculations we have an order of magnitude increase in interactions between the magnetic atoms.

4.1.7   Core d-orbitals

Photoemission spectra studies reveal that the core level spectrum of the Sn atom can be modeled by two doublets [4]. It has been debated whether these are the result of some distortion due to presence of unequal Sn atoms resulting in a 3×3 phase or due to magnetic considerations. To investigate this we calculated the DOS of the $\sqrt{3} \times \sqrt{3}$ supercell with nonmagnetic Sn atoms with relativistic considerations. This reveals a two peak structure at comparable energies to that of the experiments. Calculating the maximally localized wannier wavefunctions of the d-orbitals and plotting them reveal that the smaller of the two peaks at higher binding energy is due to the orbital $d_{x^2-y^2}$ and d_{xy} and the larger peak is due to the orbitals d_{z^2}, d_{xz} and d_{yz}. This result seems to be consistent with the geometry of the 2-d surface where the Sn orbitals extending in z direction should feel the most overlap and repulsion from the Si orbitals. Furthermore ,plotting the DOS for the AFM $2\sqrt{3} \times \sqrt{3}$ shows that the core level spectra is actually split in 4 peaks separated by very small energy differences, however as we are not able to successfully complete a magnetic calculation with relativistic considerations we are not able to capture an accurate representation of the core level in this calculation. But based on these calculations, it wouldn't be a far stretch to say that the core level spectra can be explained to be the result of predominantly geometric consideration and the doublets are a result of splitting of energy due to magnetization of the orbitals instead of the presence of a distorted 3×3 phase which is not stabilized by our DFT+U calculations.

4.2   HSE functionals [32]

Calculations using HSE functional (using 25% mixing parameter) which calculates accurate values for exchange part of the energy, was also performed in Gaussian basis set using the CRYSTAL17 package. QUANTUM ESPRESSO was not used as using HSE functional in plane wave basis set is computationally very expensive and not feasible for our calculations. Using HSE functionals in Gaussian basis set overestimated the band gap by a lot which may be due to inherent localization of the Gaussian basis set and the overestimation of the exchange part of the interaction. This is supported by the observation that decreasing the range of interaction made the band structure closer to that of PBE+U in plain wave basis set.

4.3   Doping induced Insulator-Metal transition

Following the discovery of superconductivity in hole doped 1/3 ML Sn/Si(111) [5], we tried to investigate electronic structure of the hole doped systems. We found that a doping level of 1 hole per 6 Sn atoms (16.67%) was enough to induce a transition from insulating to a conducting phase as evident by the calculated DOS (Fig. 4.9). The transition to a conducting phase is accompanied by the appearance of a van Hove singularity (VHS) peaks near -20meV which is similar to the peaks appearing in STS studies of 20% Boron doped systems (peaks near -10meV) [31]. However, there is no clear indication of spectral weight transfer to a well defined quasiparticle band as found in the experiments. We also found that the AFM phase is again the most stable phase in presence of doping compared to the paramagnetic and FM phases. This may indicate a possible coexistence of AFM magnetic order with the superconducting (SC) phase below the superconducting critical temperature.

4.4   Sample preparation and imaging

A Phosphorus doped Si(111) sample was used as the substrate. The surface was prepared it by flashing it multiple times upto 1100^0C. After the final flash the temperature was reduced to about 900^0C and then sample was annealed by slowly decreasing the temperature to 500^0C

in 30 minutes. The surface reconstruction was checked under a LEED to ascertain if we get the 7×7 reconstruction of the Si(111) surface.

Sn was evaporated on the Si substrate using an electron beam evaporator. A flux of 0.5 ML per minute was used to evaporate 1.5 ML of Sn in 3 minutes at room temperature. The surface was then annealed at around 600^0C for 2 minutes to evaporate the extra Sn atoms and obtain a 0.33 ML coverage for the $\sqrt{3} \times \sqrt{3}$ reconstruction. This was confirmed under LEED with a clear transition from the 7×7 pattern followed by a 1×1 pattern and finally the $\sqrt{3} \times \sqrt{3}$ pattern.

The prepared substrates were imaged under the STM to validate a good quality surface before deposition of the Sn adatoms. However, the STM images revealed the substrate to be full of defects and unwanted adsorbates like the presence of SiC islands. We are still in process of countering these problems and hope to get a clean surface for the Sn deposition and analysis by STS.
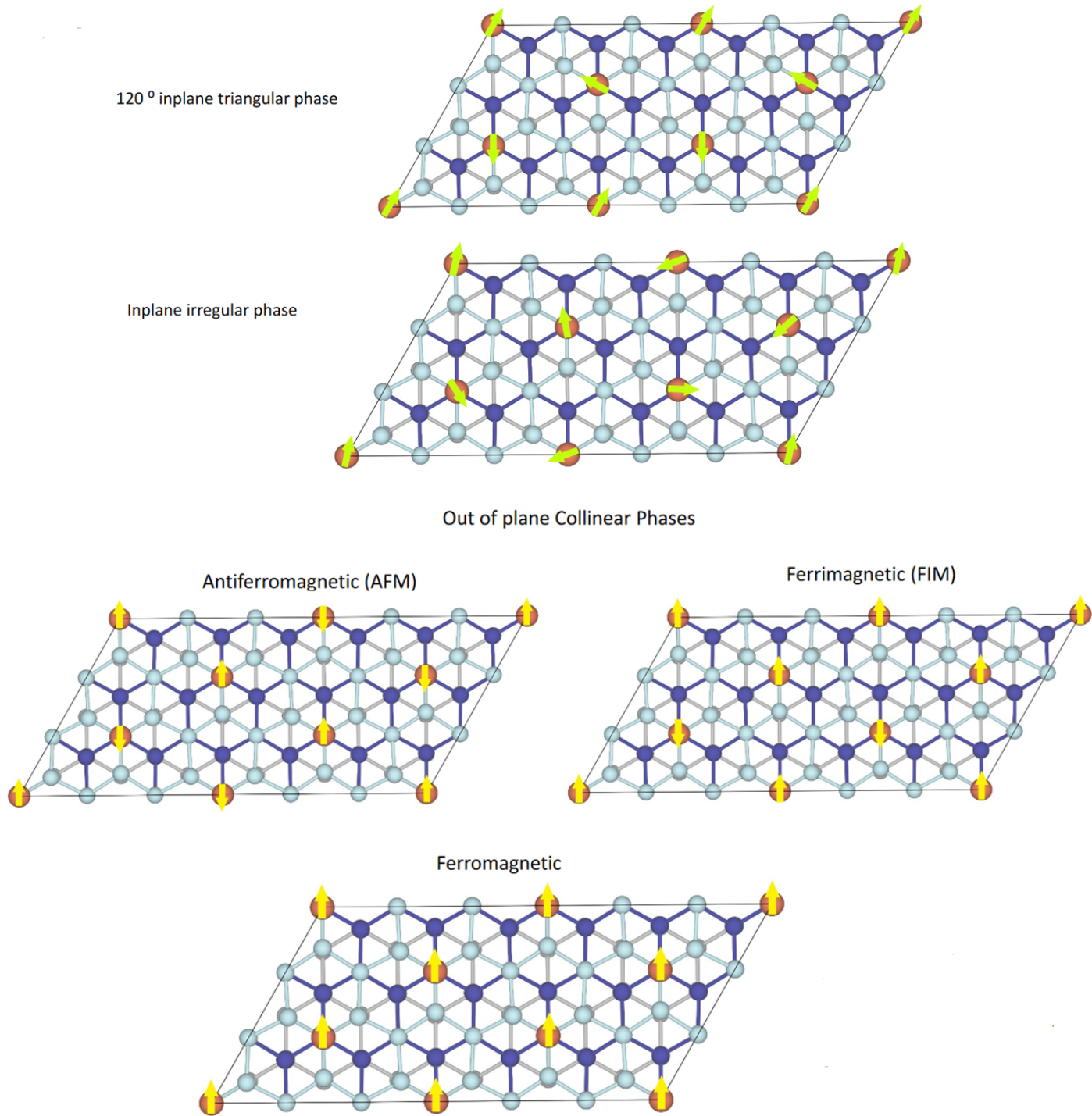
Figure 4.5: The different magnetic configurations. Top two configuration are inplane while the bottom three are out of plane magnetic moment configurations.
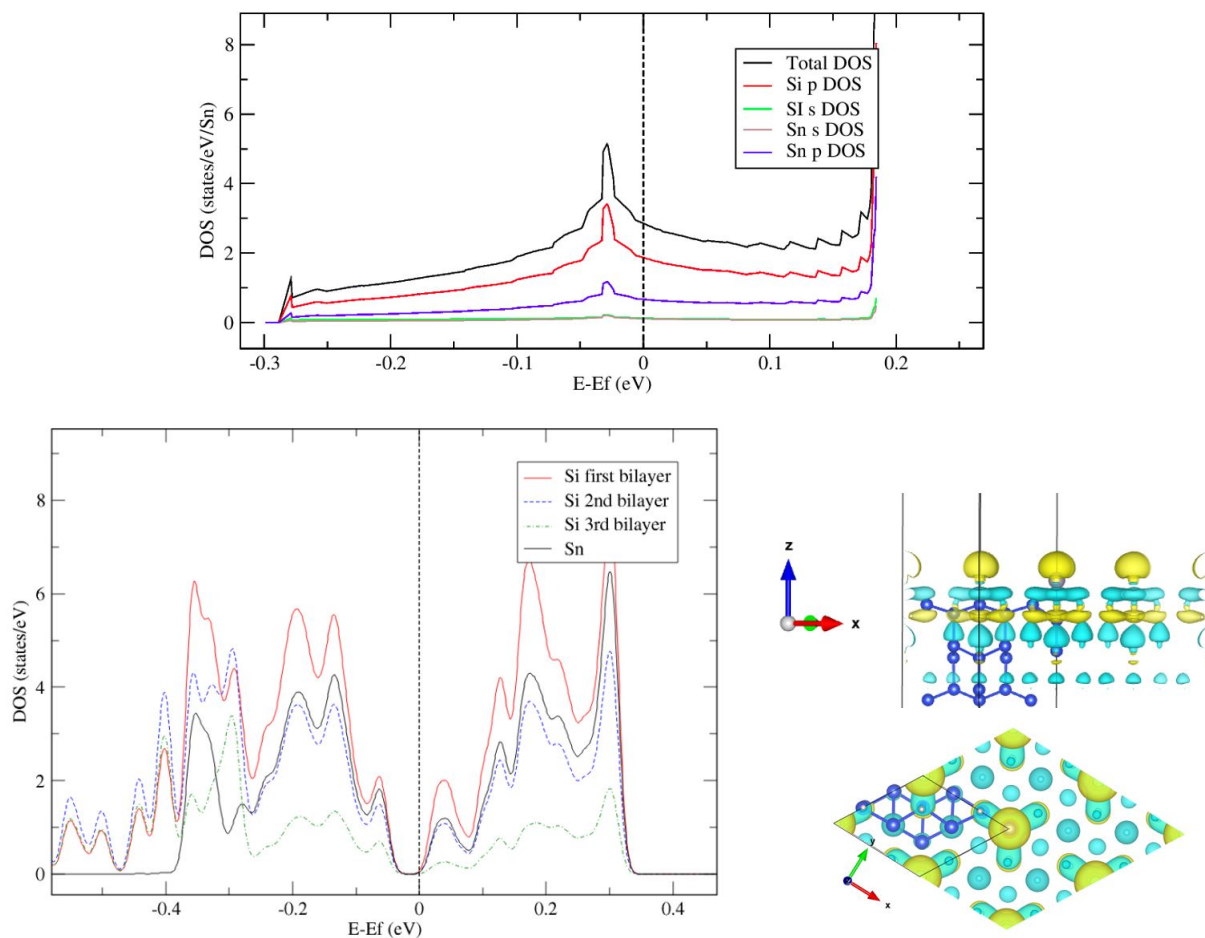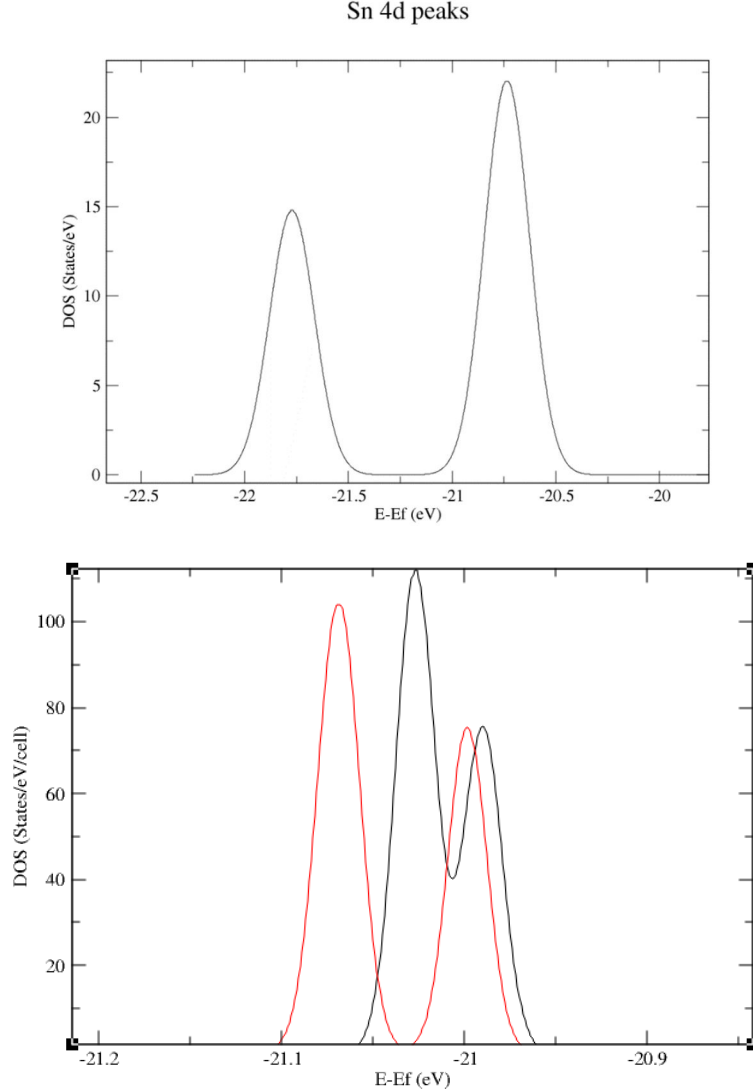
Figure 4.6: Top: The orbital resolved DOS of paramagnetic state with labeled contributions. Bottom left: DOS of AFM configuration in DFT+U resolved by the contributions coming from different layers with 15meV gaussian smoothing. Bottom right: Side and top view of Wannier functions plotted over the crystal lattice to illustrate the hybridization between layers.

Figure 4.7: Top: The dual 4d peaks in DOS of paramagnetic $\sqrt{3}x\sqrt{3}$ cell with relativistic considerations. Middle: DOS of an Sn atom in 6×3 supercell with row-wise AFM order with U=2.12 eV. We can see the the spin polaraized peaks depicted by black and red form two doublets. Bottom: The results of wannierization procedure which 2 clear group of hybridized orbitals highlighted by orange and green boxes.
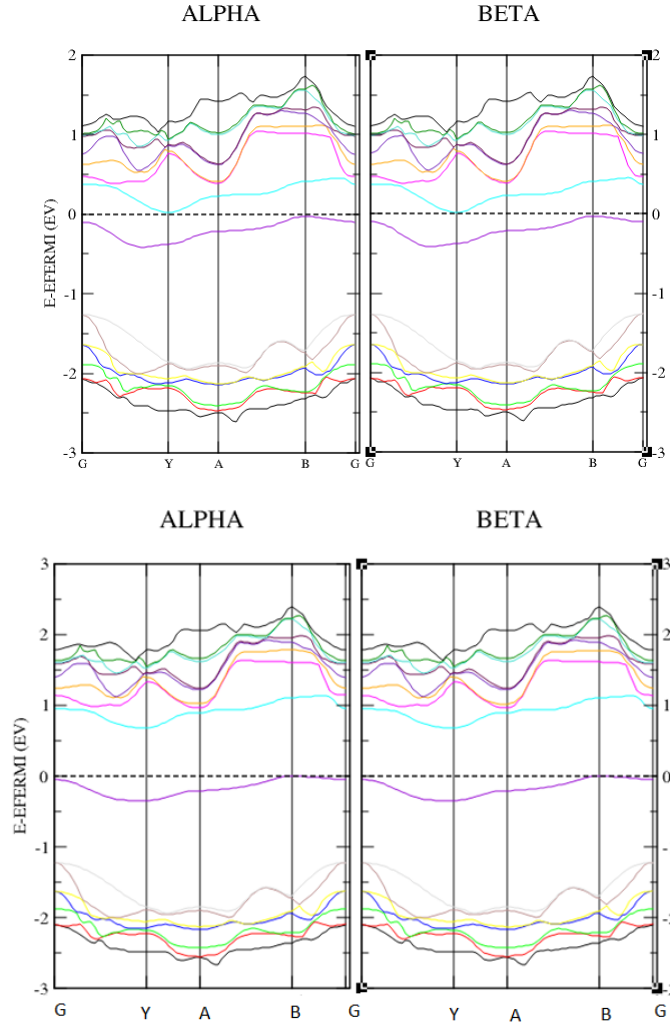
Figure 4.8: Top: HSE band structure for AFM configuration when interactions are restricted to less than 1 Å, the insulating gap is around 50meV. Bottom : HSE band structure for AFM configuration with default range of interactions, the insulating gap is around 0.7 eV. Alpha and Beta represent the two opposite spins.
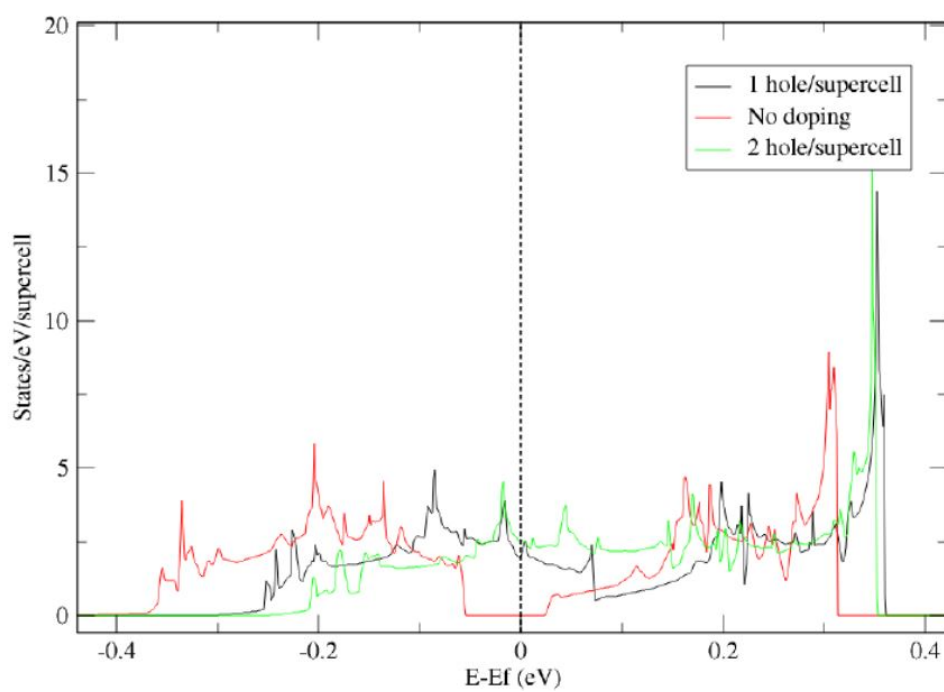
AFM hole doped Sn PDOS (6 Sn atoms/supercell)

Figure 4.9: DOS of 1 hole doped and 2 hole doped AFM configuration compared to no doping. The calculations where done in a 6×3 supercell with a Hubbard U of 2.12 eV.
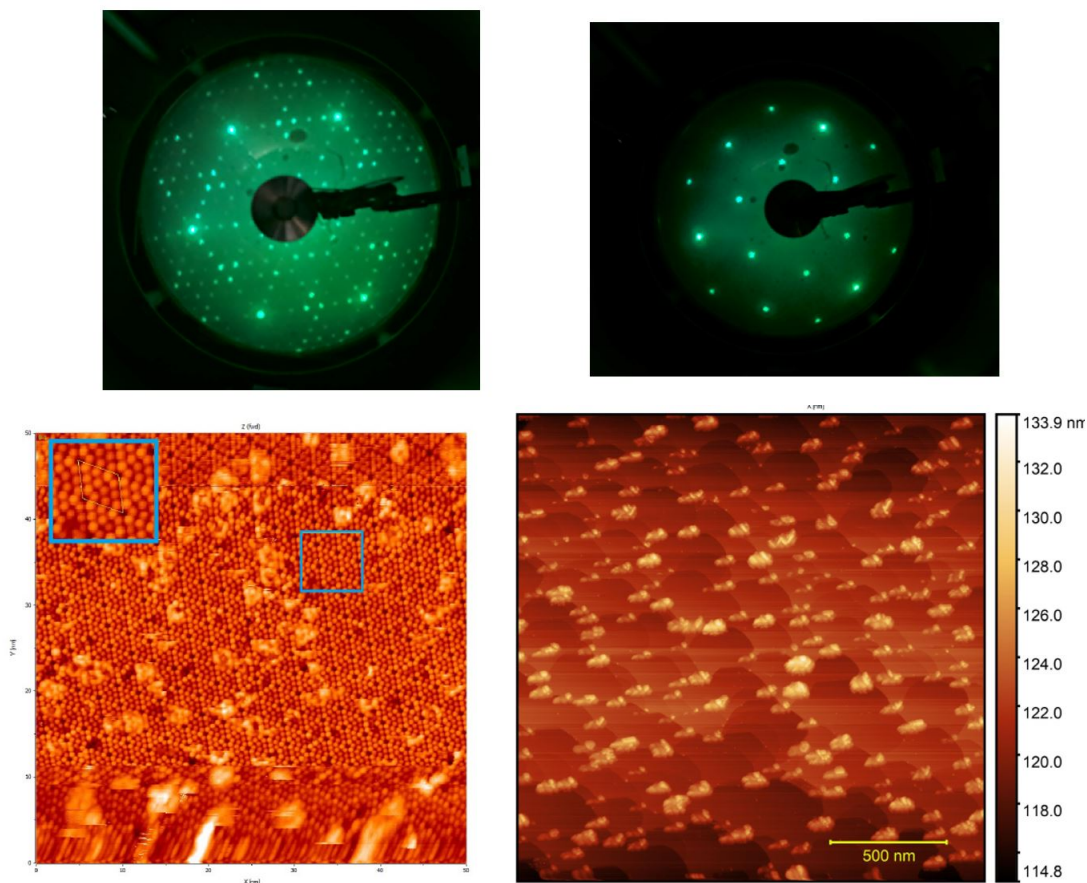
Figure 4.10: Top left : LEED image of Si(111) 7×7 surface reconstruction. Top right: LEED image of 1/3 ML Sn/Si(111) 3×3 surface reconstruction. Bottom left: A 50x50 nm image of Si(111) 7×7 surface showing various defects and impurities. The blue inset shows a zoomed in image of the boxed area with clear 7×7 cells visible. Bottom right: A large scale 2x2 μm image showing a large amount of SiC islands along the step edges.

Chapter 5

Conclusion

5.1 Discussion

Based on the DFT calculations, we are now ready to draw some conclusions keeping in mind that these are still approximations to the real system and have to be verified by careful experimentation.

The ground state appears to have the magnetic order of collinear row-wise AFM and not the 120^0 inplane triagonal order has been suggested by some. We have tried to calculate an optimal value of Hubbard U but this result may not be correct if the actual value of Coulomb repulsion is not similar to the one we calculated. This is beacause changing the value of Hubbard U can change the relative stability of the different magnetic phases.

As seen in section 4.1.5, the Sn adlayer is heavily hybridized with the Si layers underneath it which can also explain the small value of magnetization observed. This hybridization can open up the pathway for superexchange interaction of the Sn atoms via Si inspite of the Sn atoms being located far away from each other. This interaction in turn, can explain the opening up of an insulating gap in the AFM configuration in the presence of an intermediate value of U which is characteristic of a Slater type insulator. To confirm this, we will have to test if the onset of insulating behaviour coincides with the appearance of magnetic order i.e the Mott transition happens near the Neel's temperature. This also suggests that this system is not as strongly correlated as thought earlier and may not be a Mott insulator.

5.2 Future investigations and questions

Through the course of performing the calculations we have realized that the insulating gap is very small and the SOC which had been ignored earlier might influence the accuracy of the gap calculated. However, we were not able to achieve a convergence of the magnetic solution in presence of Hubbard U and SOC together. It should be interesting to see if the nature of the band changes in presence of SOC in the future.

A large part of this project involving experimental measurements using scanning tunneling spectroscopy (STS) could not be performed in time due to various technical difficulties with the setup. We hope to investigate the predictions of the thesis in near future experiments.

We were also able to obtain isoenergy images and joint density state(JDOS) plots for the surface of the system using Wannier wavefunctions and we hope to analyze these images and compare it to future experimental results.
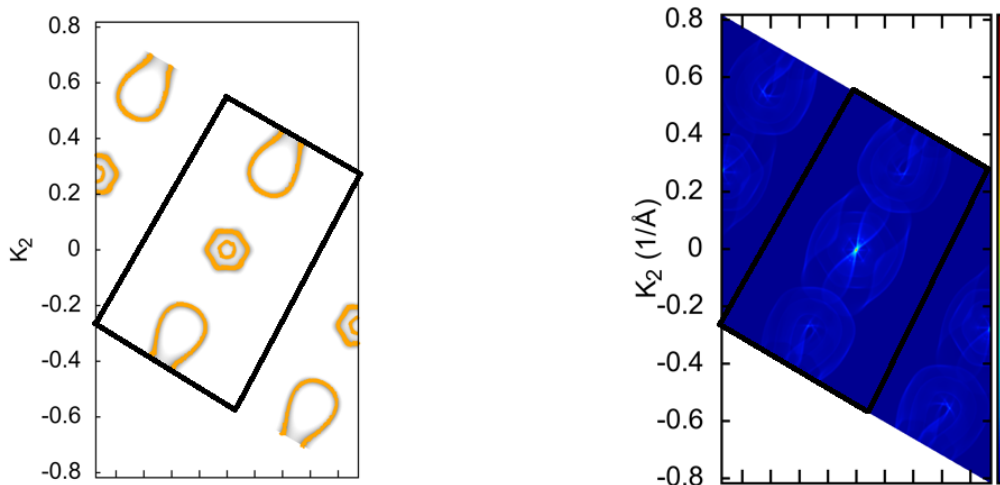

Figure 5.1: Isoenergy surface and joint DOS of the DFT+U AFM calculation at -50meV energy. The black box represents the brillouin zone of $2\sqrt{3} \times 3$ periodic cell which houses the row-wise AFM order.

The very interesting claim of unconventional 2-D superconductivity in doped 1/3 ML Sn/Si [5] is sure to be followed up by a lot of work in such correlated materials. We have done a brief investigation of the insulator to metal transition in presence of hole doping as

discussed in 4.3. We could not go to lower doping levels due to being constrained with the size of the supercell. A lower doping level would require a bigger cell and higher computational cost. We hope that future studies can help characterise the transition point of the insulator to metal transition as a function of doping. Furthermore, it will also be interesting to see if we are able to calculate the properties of the superconductor using DFT or the system is truly governed by strong electronic correlations instead of electron-phonon interactions so that DFT is unable to capture the physics of the superconductor.

Bibliography

[1] Bednorz, J. G.; Müller, K. A. (1986). "Possible high TC superconductivity in the Ba-La-Cu-O system". Zeitschrift für Physik B. 64 (2): 189–193

[2] Novoselov, K. S.; Geim, A. K.; Morozov, S. V.; Jiang, D.; Zhang, Y.; Dubonos, S. V.; Grigorieva, I. V.; Firsov, A. A. (22 October 2004). "Electric Field Effect in Atomically Thin Carbon Films". Science. 306 (5696): 666–669.

[3] M. Jäger, C. Brand, A. P. Weber, M. Fanciulli, J. H. Dil, H. Pfnür, and C. Tegenkamp Phys. Rev. B 98, 165422

[4] Modesti et al. (2007). Insulating ground state of Sn/Si(111)-(square root 3 x square root 3)R30 degrees.. Physical review letters. 98. 126401

[5] Xuefeng Wu et al, Superconductivity in a hole-doped Mott-insulating triangular adatom layer on a silicon surface, https://arxiv.org/ftp/arxiv/papers/1912/1912.03242.pdf

[6] Estefania German et al 2017 J. Phys. Commun.1 055006

[7] Juarez L. F. Da Silva Phys. Rev. B 76, 193108

[8] Hohenberg, Pierre; Walter, Kohn (1964). "Inhomogeneous electron gas". Physical Review. 136 (3B): B864–B871.

[9] Kohn, W.; Sham, L. J. (1965). "Self-consistent equations including exchange and correlation effects". Physical Review. 140 (4A): A1133–A1138.

[10] John P. Perdew; Matthias Ernzerhof; Kieron Burke (1996). "Rationale for mixing exact exchange with density functional approximations" (PDF). J. Chem. Phys. 105 (22): 9982–9985.

[11] Martin, R., 2004. Electronic Structure: Basic Theory And Practical Methods. Cambridge University Press, p.173.

[12] de Boer, J. H.; Verwey, E. J. W. (1937). "Semi-conductors with partially and with completely filled 3d-lattice bands". Proceedings of the Physical Society. 49 (4S): 59

[13] Mott, N. F.; Peierls, R. (1937). "Discussion of the paper by de Boer and Verwey". Proceedings of the Physical Society. 49 (4S): 72.

[14] A. Georges; G. Kotliar; W. Krauth; M. Rozenberg (1996). "Dynamical mean-field theory of strongly correlated fermion systems and the limit of infinite dimensions". Reviews of Modern Physics. 68 (1): 13.

[15] arXiv:cond-mat/9903273 [cond-mat.str-el]

[16] M Cococcioni, "The LDA+U Approach: A Simple Hubbard Correction for Correlated Ground States", Correlated Electrons: From Models to Materials Modeling and Simulation Vol. 2 Forschungszentrum Julich, 2012, ISBN 978-3-89336-796-2

[17] M. Cococcioni and S. de Gironcoli, Phys. Rev. B71, 035105 (2005)

[18] S.L. Dudarev, G.A. Botton, S.Y. Savrasov, C.J. Humphreys, and A.P. Sutton,Phys. Rev. B57, 1505 (1998)

[19] J.P. Perdew and M. Levy, Phys. Rev. Lett.51, 1884 (1983)

[20] M. Levy, Phys. Rev. A26, 1200 (1982)

[21] G. Profeta and E. Tosatti, Phys. Rev. Lett.98, 086401(2007).

[22] Kittel, C. (1976). Introduction to Solid State Physics, New York: John Wiley Sons.

[23] Ewald, P. P. (1969). "Introduction to the dynamical theory of X-ray diffraction". Acta Crystallographica Section A. 25 (1): 103–108.

[24] I. Horcas, R. Fernandez, J.M. Gomez-Rodriguez, J. Colchero, J. Gomez-Herrero and A. M. Baro, Rev. Sci. Instrum. 78, 013705 (2007)

[25] Yi, S., Lee, H., Choi, J. et al. "Nature of the Insulating Ground State of the Two-Dimensional Sn Atom Lattice on SiC(0001)". Sci Rep 6, 30598 (2016).

[26] A. Mascaraque, J. Avila, J. Alvarez, M. C. Asensio, S. Ferrer, and E. G. Michel, "Nature of the Low-Temperature 33 Surface Phase of Pb/Ge(111)", Phys. Rev. Lett. 82, 2524(1999)

[27] C. Tresca, C. Brun, T. Bilgeri, G. Menard, V. Cherkez, R. Federicci, D. Longo, F. Debontridder, M. D'angelo, D. Roditchev, G. Profeta, M. Calandra, and T. Cren, Chiral, "Spin Texture in the Charge-Density-Wave Phase of the Correlated Metallic Pb/Si(111) Monolayer", Phys. Rev. Lett. 120, 196402(2018)

[28] R. Cortés, A. Tejeda, J. Lobo-Checa, C. Didiot, B. Kierren, D. Malterre, J. Merino, F. Flores, E. G. Michel, and A. Mascaraque, Phys. Rev. B 88, 125113 (2013)

[29] A. B. Odobescu, A. A. Maizlakh, N. I. Fedotov, and S. V. Zaitsev-Zotov, Phys. Rev. B 95, 195151

[30] P Giannozzi et al, J.Phys.:Condens.Matter 29, 465901 (2017)

[31] F Ming et al, "Realization of a Hole-Doped Mott Insulator on a Triangular Silicon Lattice", Phys. Rev. Lett. 119, 266802 (2017)

[32] Jochen Heyd; Gustavo E. Scuseria; Matthias Ernzerhof (2003). "Hybrid functionals based on a screened Coulomb potential". J. Chem. Phys. 118 (18): 8207.

[33] By Jatosado - Power Point, CC BY-SA 3.0, https://commons.wikimedia.org/w/index.php?curid=20419103

[34] Gerbald. M. "2D superconductors perturbed by local magnetism: from Yu-Shiba Rusinov bound states to Majorana quasiparticles". Phd thesis, 2016.

[35] Wannier90 as a community code: new features and applications, G. Pizzi et al., J. Phys. Cond. Matt. 32, 165902 (2020)